Journal of Nuclear Materials 408 (2011) 161–170

Contents lists available at ScienceDirect

Journal of Nuclear Materials

journal homepage: www.elsevier.com/locate/jnucmat

# Segregation of Cr at tilt grain boundaries in Fe–Cr alloys: A Metropolis Monte Carlo study

D. Terentyev [a,*], X. He [a,b], E. Zhurkin [c], A. Bakaev [a,c,d]

[a] SCK.CEN, Structural Materials Group, Nuclear Materials Science Institute, B-2400 Mol, Belgium
[b] China Institute of Atomic Energy, P.O. Box 275-51, 102413 Beijing, China
[c] Experimental Nuclear Physics Department, K-89, Faculty of Physics and Mechanics, Saint-Petersburg State Polytechnical University, 29 Polytekhnicheskaya str., 195251 St. Petersburg, Russia
[d] Center for Molecular Modeling, Ghent University, Proeftuinstraat 86, B-9000 Gent, Belgium

ARTICLE INFO

*Article history:*
Received 7 June 2010
Accepted 11 November 2010

ABSTRACT

In this work, the Metropolis Monte Carlo (MMC) method employing the isothermal–isobaric statistical ensemble is applied to investigate segregation at grain boundaries in bcc Fe–Cr alloys with varying Cr content from 5 to 14 at.%. Several different ⟨1 1 0⟩ tilt grain boundaries, namely: Σ19{3 3 1}, Σ9{2 2 1}, Σ3{1 1 1}, Σ3{1 1 2}, Σ11{1 1 3}, Σ9{1 1 4} with misorientation angle varying in the range 26–141° were considered. Systematic MMC simulations were performed employing a two band empirical many-body potential in the temperature range 300–900 K. It was found that the binding energy of substitutional Cr to the GB core is essentially determined by the structure of the GB interface and varies in the range 0.05–0.35 eV. At this, the binding energy increases with the GB excess volume. MMC simulations revealed that either a local atomic rearrangement or segregation of Cr at the considered GBs occurs depending on the combination of temperature, alloy composition and GB structure. Influence of temperature and GB structure on the local atomic rearrangement and precipitation of $\alpha'$ particles is demonstrated.



## 1. Introduction

Segregation of alloying elements to grain boundaries in binary alloys or complex compounds may alter their structure and local chemical composition, which in turn changes mechanical properties of the material, for instance its fracture behavior [1]. Segregation can be induced by thermal annealing or/and irradiation, which offers additional means for the mass transport and can cause non-equilibrium segregation [2]. This is why grain boundary (GB) segregation has been extensively studied over the last few decades both experimentally and theoretically. Recently, a significant part of theoretical investigations was focused on atomistic computer simulations, which is a powerful tool to gain knowledge about GB structure, cohesive and mechanical properties at the atomic level. However, the segregation in concentrated alloys was mainly studied in face centered cubic (FCC) systems such as Cu–Ag and Ni–Al (see e.g., [3,4]). Little work has been done so far in body centered cubic (BCC) concentrated alloys.

The present work focuses on the study of tilt grain boundaries in bcc Fe–Cr disordered alloys with Cr content in the range 5–14 at.% Cr. The latter alloys are often considered as model alloys for ferritic/martensitic (F/M) steels (including reduced activation steels [5]), which are commonly used as structural materials for gas turbines and nuclear power systems. This choice was made based on superior mechanical properties and good resistance to neutron irradiation. The segregation/precipitation of Cr in bcc Fe–Cr alloys and steels containing more than 13 at.% Cr is long known to cause embrittlement during thermal ageing in the temperature range 400–550 °C. For instance, enrichment of Cr at grain boundaries under thermal ageing of Fe–Cr alloys containing more that 13 at.% Cr was reported by Lagneborg [6]. Experiments involving irradiation in Fe–13Cr [7] and Fe–10Cr [8] alloys show that Cr depletion takes place after electron irradiation at 400° and 500 °C, respectively. Whereas, in Fe–2.8Cr, a strong enrichment was observed under electron irradiation at 600 °C [9]. Finally, neither enrichment nor depletion of Cr was seen in Fe–5Cr alloy irradiated at 400 °C [7]. Summary of other experimental works involving irradiation can be found in Ref. [10], which points out that there is no clear indication for radiation induced segregation or depletion of Cr. It is important to note that the sign of the heat of mixing of Fe–Cr changes from negative to positive at about 9% Cr [11]. As a result, Cr atoms in the alloys containing more than 10% Cr tend to precipitate (see e.g., [6,12,13]), and otherwise tend to order [14]. Up to now very little is known about how the presence of the GB region may locally alter phase separation or ordering in Fe–Cr alloys, depending on temperature and GB structure. These issues are the subject of the current work.

* Corresponding author. Tel.: +32 14 333197; fax: +32 14 321216.
*E-mail address:* dterenty@sckcen.be (D. Terentyev).

0022-3115/$ - see front matter © 2010 Elsevier B.V. All rights reserved.
doi:10.1016/j.jnucmat.2010.11.024

One of the common numerical methods to study equilibrium GB segregation is the Metropolis Monte Carlo (MMC) method [15], which allows a variation of the volume, pressure and chemical potential, and to include atomic relaxations, while approaching the equilibrium state [16]. Another advantage of this method is that it can handle relatively large systems containing up to few hundred thousands of atoms. In the present work we apply the MMC method to study rearrangement of Cr atoms near different ⟨1 1 0⟩ tilt GBs in Fe–*x*Cr alloys at thermodynamic equilibrium. The concentration of Cr, $x$ = 5, 10, 14 at.%, was chosen to cover a typical range of Cr content in the F/M steels for nuclear application. GBs selected were intended to span a wide range of structures with essential variation in GB energy, structure and excess volume.

## 2. Computational details

### 2.1. MMC simulations

MMC sampling was realized within the isobaric–isothermal (*NPT*) statistical ensemble where $N$ is the number of particles, $P$ is the pressure and $T$ is the temperature, which are kept constant during simulation runs. Three different types of trials were considered, namely: (i) random displacement of any atom from its position (by this trial, lattice relaxation and vibrational entropy are accounted for); (ii) swapping of atoms of different kinds, selected at random; (iii) overall volume change of the simulation box to maintain a desired pressure. The decision on the acceptance of a newly obtained configuration for the first two trials is based on the ratio of the probabilities as follows [17,18]:

$$P_{new}/P_{old} = min\{1, exp(-\Delta E/k_BT)\} \quad (1)$$

where $k_BT$ is the Boltzmann factor, and $\Delta E$ is the difference between the total energy of the old and new configurations. A step involving the first two trials is repeated until all atoms in the box have undergone the displacement and exchange several times. Then, the lattice parameter along one of the randomly selected Cartesian box directions is changed at random and the relative probability for the acceptance is determined as:

$$P_{new}/P_{old} = exp\{-(\Delta E + P\Delta V - NkT\Delta lnV)/k_BT\} \quad (2)$$

where $V$ is the box volume. The acceptance criterion ensures a convergence of the pressure to a given value. One set of these three trials will be referred to as a 'macrostep'. The establishment of the equilibrium was based on several criteria such as the convergence of the total energy, dimensions of the system and the short range order parameter, calculated for Fe–Cr pairs within the second nearest neighbour distance in bcc lattice. Typically, at least one million macrosteps were sampled to achieve a convergence. The final configurations subject to analysis were obtained by averaging the atomic position and chemical type of each atom over the last million of macrosteps, once the steady-state was reached (typically after a few millions of macrosteps). All MMC simulations were performed applying 3D periodic boundary conditions, obeying zero pressure during the run. The present simulations were performed in bcc Fe–Cr alloys containing 5, 10 and 14 at.% Cr at $T$ = 300, 600 and 900 K. The initial spatial distribution of Cr in the model boxes was selected at random, while the initial atomic positions were obtained after molecular static (MS) relaxation in pure Fe, performed as described in the following.

### 2.2. Molecular static simulations

MS calculations have been performed with supercells containing two grains of bcc Fe. A GB bisects the model and is periodic in the plane of the GB and perpendicular to it. The following symmetric tilt grain boundaries with a common ⟨1 1 0⟩ tilt axis were considered: Σ19{3 3 1}, Σ9{2 2 1}, Σ3{1 1 1}, Σ3{1 1 2}, Σ11{1 1 3}, Σ9{1 1 4}. In what follows we shall omit the notation 'Σ' and specify each GB referring to its plane orientation only. The above listed GBs were prepared considering mirror symmetry for the bi-crystals. All details about relaxation procedure and construction of the GBs are described in Ref. [19] and here we only briefly recall the main points. The initial separation between two layers belonging to the different grains was set to that inside the grains. Ground state structures for each GB were determined by computing the $\gamma$-surface. Once the global energy minimum is identified we apply rigid-body translations of the grains and perform the full relaxation of the crystal to find an optimum spacing perpendicular to the GB plane. This was done by applying periodic boundary conditions along $x$ (tilt axis) and $y$ (normal to the tilt axis) directions and free surface normal to the GB plane ($z$ axis). The movement of atoms in the few surface layers was constrained in the $z$ direction. The selected shift and optimal spacing were then used to construct 3D periodic crystals and relax them again. A summary of the properties of the GBs and geometrical sizes of the simulation cells used in the MMC simulations are reported in Table 1. The relaxed structures of the studied GBs are shown in Fig. 1, where a dotted line shows the position of the GB plane and a solid line connects atoms forming an identical structural unit. In our previous work, the ground state configurations of these GBs were discussed in terms of the deviation of atomic positions as compared to the perfectly symmetric structures [19]. For the currently used Fe–Fe interatomic potential it was found that for all GBs, very little or no relaxation at all occurs along the tilt axis. For the {1 1 1} GB only displacements perpendicular to the GB plane occurred, whereas for the {1 1 2} GB only in-plane (shear) displacements were found. The strong relaxations in the $yz$ plane (i.e., perpendicular to the tilt axis) were seen in the {1 1 3}, {1 1 4} and {3 3 1} GBs. At this, the relaxations in the {3 3 1} GB actually induced a small contraction of a cell along the $z$ axis, which was not observed for other studied GBs. Considering the elementary structures of the GBs shown in Fig. 1, it is clear that only the {1 1 2} and {1 1 3} GBs have shifted configurations, whereas the rest are perfectly symmetric.

**Table 1**
Characteristics of ⟨1 1 0⟩ tilt grain boundaries with different misorientation angles ($\varphi$) calculated in pure Fe. The GB energy is given for the fully relaxed structure (see text for details). Available *ab initio* data ([*],[**]) are added for comparison.

| GB type | $\varphi$ (°) | Crystal size, $a_0 \times a_0 \times a_0$ | $\gamma_{GB}$ (J/m$^2$) | Number of atoms | Excess volume/GB area (Å) | Maximum value of $E_B$ (eV) |
|---|---|---|---|---|---|---|
| Σ9{2 2 1} | 38.94 | 43.8 × 42.0 × 28.8 | 1.1674 | $10.32 \times 10^4$ | 0.364 | 0.33371 |
| Σ19{3 3 1} | 26.53 | 43.8 × 43.58.0 × 28.2 | 1.44566 | $10.72 \times 10^4$ | −0.01 | 0.26726 |
| Σ3{1 1 1} | 70.53 | 43.8 × 36.74 × 27.8 | 1.2952 (1.57[*]) (1.52[**]) | $8.93 \times 10^4$ | 0.402 | 0.19817 |
| Σ3{1 1 2} | 109.47 | 43.8 × 41.56 × 28.02 | 0.26155 (0.34[**]) | $10.11 \times 10^4$ | 0.002 | 0.04863 |
| Σ11{1 1 3} | 129.52 | 43.8 × 43.11 × 28.1 | 1.58167 | $10.47 \times 10^4$ | 0.383 | 0.18056 |
| Σ9{1 1 4} | 141.06 | 43.8 × 42.42 × 28.12 | 1.2858 | $10.41 \times 10^4$ | 0.352 | 0.33096 |

[*] E. Wachowicz, T. Ossowski, A. Kiejna, Physical Review B 81 (2010) 094104.
[**] H. Nakashima, M. Takeuchi, Iron Steel Inst. Japan (ISIJ) 86 (2000) 357.

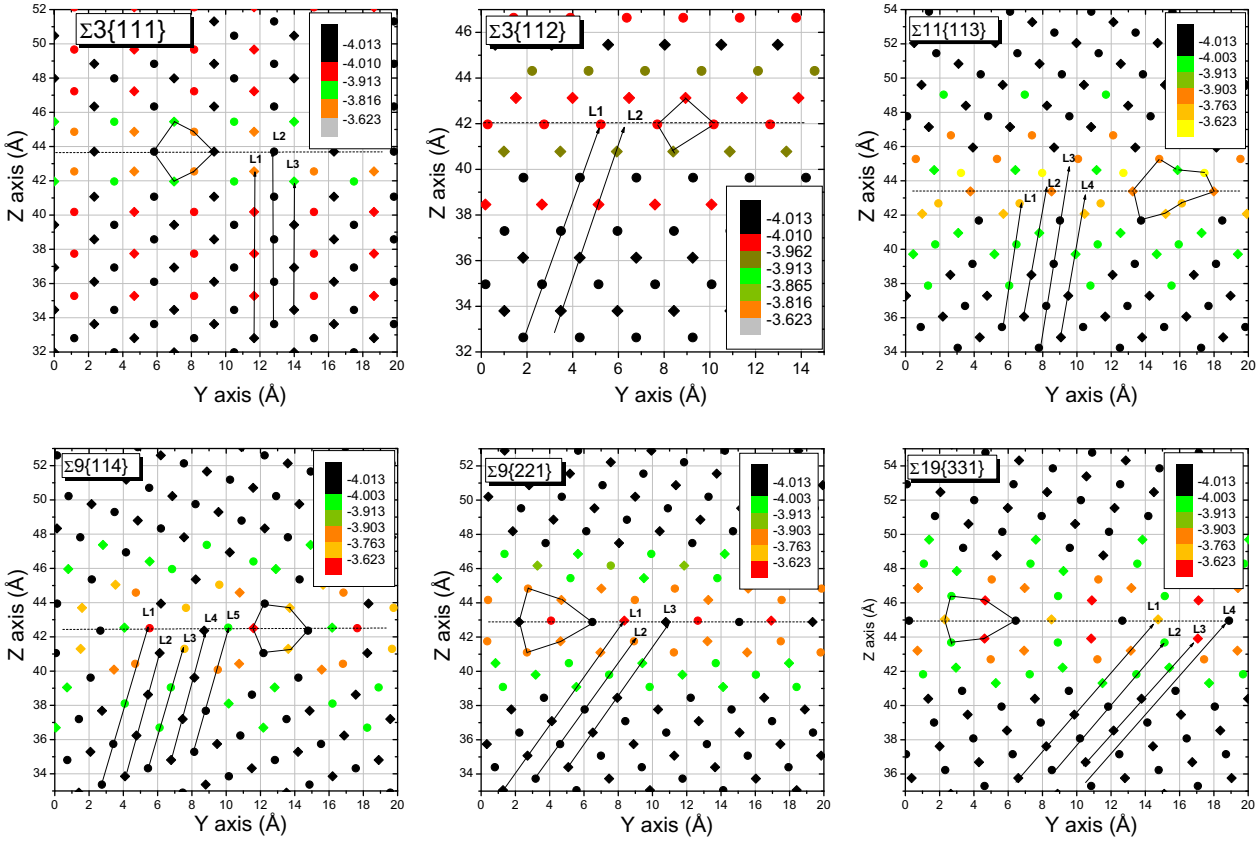


**Fig. 1.** Atomic structures of the studied ⟨1 1 0⟩ tilt GBs obtained after MS relaxation. Atomic positions in two non-equivalent {1 1 0} planes are shown by filled circles and squares, respectively. The inset colour scale specifies the potential energy of Fe atoms. Lattice sites where a substitutional Cr atom was inserted to calculate the interaction energy are shown by arrows labeled as $L_{1,2,\ldots,5}$.

The interaction of a Cr atom with the GBs was studied by insertion of a single Cr atom in a substitutional position, and then relaxing the simulation block to reach the convergence of the force per atom of 0.01 eV/Å. Lattice sites where a substitutional Cr atom was inserted are shown in Fig. 1 by arrows labeled as $L_{1,2,\ldots,5}$. The binding energy of Cr with a given GB, $E_B$, is determined as the difference of the total energy of the crystal when Cr is present far away and nearby the GB core. With this notation, a positive value of $E_B$ means an attractive interaction.

To describe the Fe–Cr system, we have opted for the two band model potential developed in Ref. [20], which was extensively used in the past few years to model properties of lattice defects, dislocations, to describe primary damage and phase separation in the Fe–Cr system (see e.g., Refs. [21–26] and references sited therein). The Fe–Fe part of this potential is the one derived by Ackland et al. in 2004 [27], which is significantly improved compared to the previously existing Fe–Fe many-body potentials in terms of description of self-interstitial defects and dislocation properties, as was validated using *ab initio* calculations [28,29]. The Fe–Cr potential was validated using *ab initio* calculations with respect to Cr–Cr interaction in the bulk, Cr-point defect interaction [30].

## 3. Results and discussion

### 3.1. Static calculations

The binding energy for a substitutional Cr atom versus distance from the GB interface in pure Fe is shown in Fig. 2 and the maximum binding energy is reported in Table 1 for each GB. The binding energy shown in Fig. 2 was calculated for all lines shown in Fig. 1 and then sorted by the distance between a Cr atom and GB interface. We can see that Cr is strongly attracted to all GBs except for the 112 GB, for which the maximum binding energy is only ~0.05 eV. In general, the maximum binding energy increases with the GB excess volume, which is also reported in Table 1. The exception is the 331 GB, for which the negative excess volume is found and still a relatively high binding energy is present. Near the GB core the interaction energy is highly non-uniform i.e., it changes significantly depending on a specific lattice site into which a Cr atom is inserted. In addition, occupation of some lattice sites in the GB core by Cr is not energetically favourable. Thus, the difference in the binding energy for the favourable and unfavourable neighbouring sites can go up to 0.5 eV, which is the case of the 221 and 331 GB. The smoothest binding energy profile is obtained for the 112 GB, which also exhibits the weakest interaction with a substitutional Cr atom. The strongest attraction of Cr to the GB core ($E_B$ = 0.25 − 0.33 eV) is observed for the 114, 221 and 331 GBs. Finally, we mention that the binding energy approaches zero at a distance of about 0.6 nm from the GB, irrespective of its type (see Fig. 2).

The observed attraction of substitutional Cr to the GB core qualitatively agrees with the results obtained from *ab initio* calculations [31], where Σ3{1 1 1}⟨1 1 0⟩ and Σ5{2 1 0}⟨0 0 1⟩ were studied. For both of these GBs the presence of a substitutional Cr atom in the GB core was found to be energetically favourable. A direct comparison of the present results and those published in [31] is not possible because the concentration of Cr per atomic layer in [31] was 50% or 25% for the two crystals used in the *ab initio* calculations.

### 3.2. MMC calculations

The atomic configurations obtained after MMC simulations were analyzed in terms of Cr concentration profile along the nor-

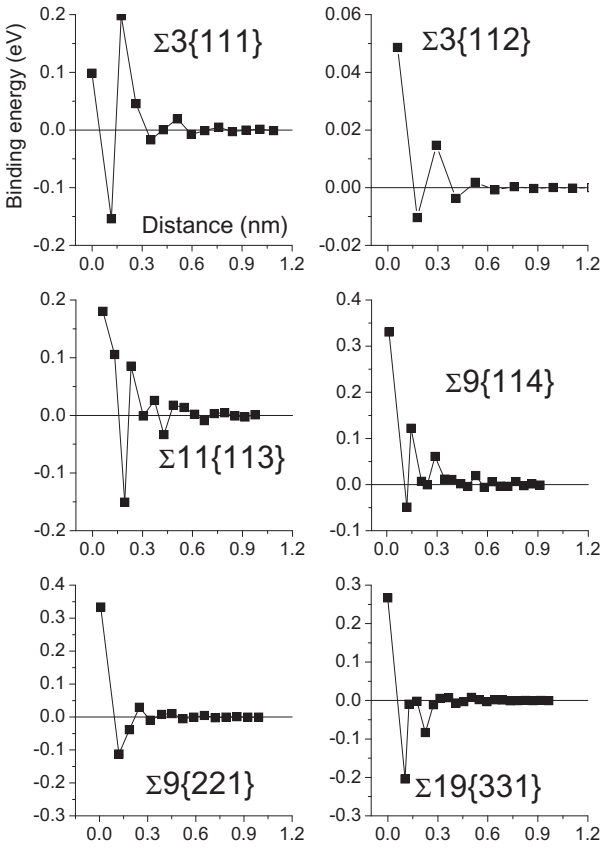


**Fig. 2.** Binding energy of a substitutional Cr as a function of distance to the GB core.

mal to the GB plane, short range order parameter, change of the GB energy and structure. Let us first discuss the concentration profiles, which are shown in Figs. 3–5 as a stack of plots obtained for each GB in Fe–5Cr, Fe–10Cr and Fe–14Cr alloys, respectively. The profiles were constructed by calculating Cr concentration in slices of a width of $a_0$, which is ~0.28 nm (depending on Cr composition and temperature). In most of the plots the segregation of Cr was expressed as a peak in the middle or near the edge of the $z$ axis (due to periodic boundary conditions imposed). Thus, we can clearly ascribe this to the Cr enrichment at the GB core. The main effect of temperature is to reduce the enrichment (if it occurred) but not to modify the structure of the profile. The role of alloy composition and GB type is much more prominent. We, therefore, shall describe the main features of the profiles shown in Figs. 3–5 for each alloy separately. We also calculated the amount of segregation, $\Delta_S$, which is a difference between Cr content contained within the GB core (the slice corresponding to the position of the GB plane) and nominal Cr concentration. These data are presented in Fig. 6.

Prior to describe the results for each alloy separately, it is useful to remind the solubility limit for the studied compositions, obtained with the applied here potential. Cr is fully soluble in Fe–5Cr at 300 K and above, in Fe–10Cr above 550 K and in Fe–14Cr Cr above ~800 K [32]. Considering the temperature interval studied here, the equilibrium phase separation should occur at 300 K in Fe–10Cr, Fe–15Cr alloys, and at 600 K only in Fe–14Cr.

In Fe–5Cr alloy, the enrichment of Cr at the GB core was found in all the GBs except for the 112. Strong segregation in and sharp depletion outside the core of the 114, 221 and 331 GBs was observed at all temperatures. In the case of the 111, 112 and 113 GBs only a moderate Cr enrichment occurred. Snapshots showing positions of Cr atoms in the bi-crystals containing 112 and 221 GBs obtained from the MMC simulations at 600 K are presented in Fig. 7a and b, respectively. We can clearly see that in the 221 GB, the core containing two atomic layers is enriched by Cr, while the two nearest layers almost do not contain Cr. In contrast to this, the distribution of Cr in the 112 GB is more or less homogenous. Increasing temperature up to 900 K leads to the disappearance of Cr enrichment only at 111, 112 and 113 GBs, whereas other GBs remain enriched (see Fig. 6a).

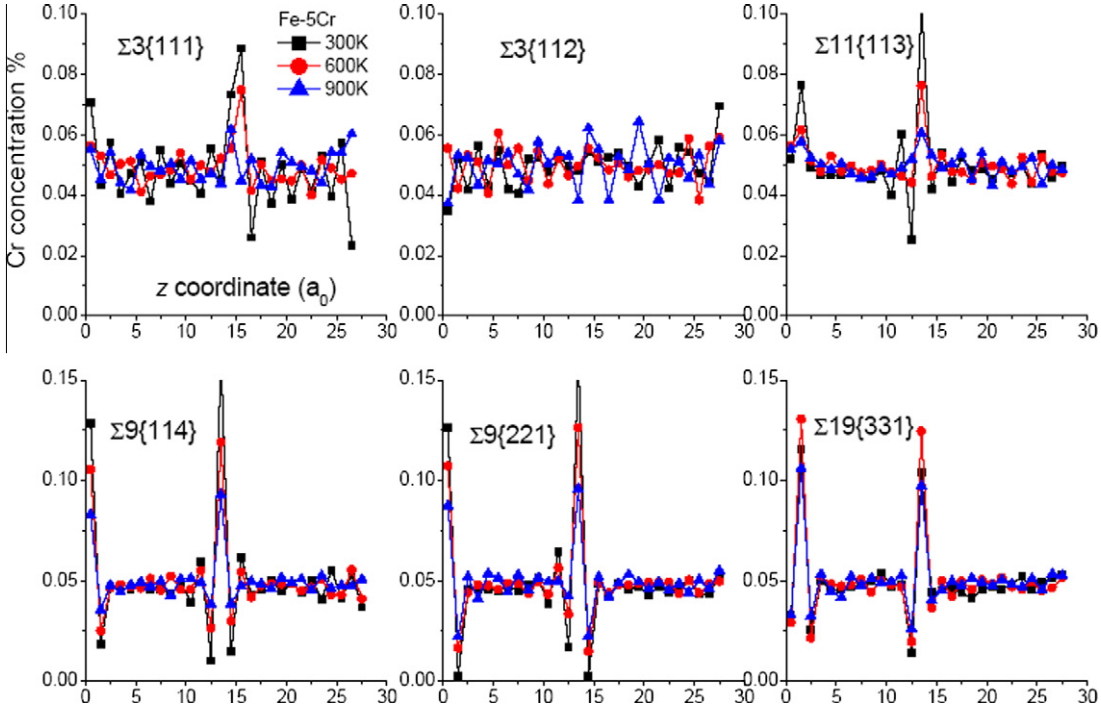


**Fig. 3.** Concentration profiles of Cr in the Fe–5Cr bi-crystals after MMC simulations at $T$ = 300, 600, 900 K.

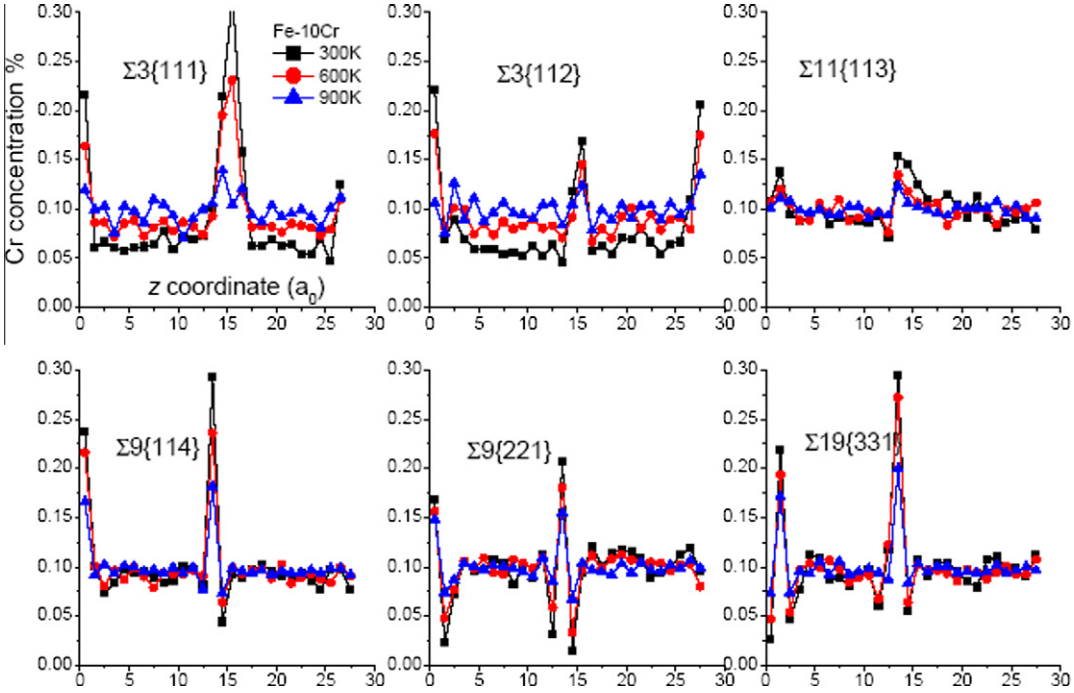


**Fig. 4.** Concentration profiles of Cr in the Fe–10Cr bi-crystals after MMC simulations at $T$ = 300, 600, 900 K.

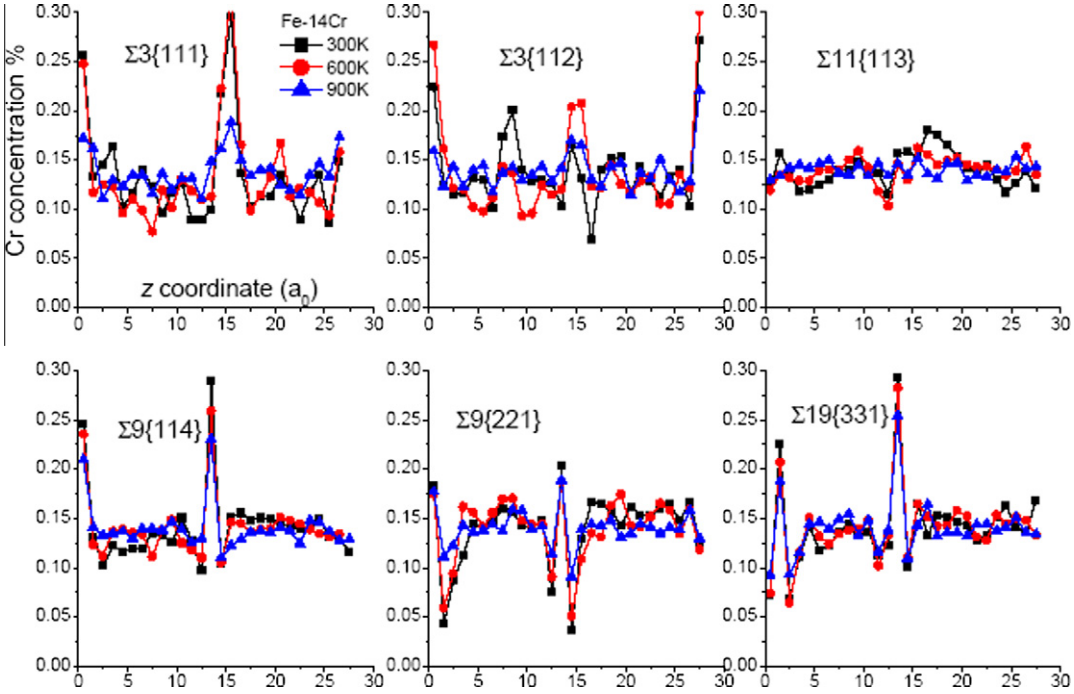


**Fig. 5.** Concentration profiles of Cr in the Fe–14Cr bi-crystals after MMC simulations at $T$ = 300, 600, 900 K.

The enrichment of the GB core in the Fe–10Cr bi-crystals was more pronounced, see Figs. 4 and 6b. This time, however, very weak enrichment was seen in the core of the 113 GB, irrespective of the simulation temperature. A local depletion was again observed near the core of the 114, 221 and 331 GBs just as in Fe–5Cr alloys. In all the considered GBs the enrichment of Cr essentially decreases with temperature, but the strongest effect is again seen in the case of the 111, 112 and 113 GBs. In simulations performed at 300 K, a new feature not observed in Fe–5Cr was revealed. In the 111 and 112 GBs, the matrix contained between the two GB interfaces was seen to be depleted with Cr (see Fig. 4). The average content of Cr in the matrix was ~6%. With increasing temperature up to 600 K (above the miscibility gap for the $\alpha$–$\alpha'$ separation) this depletion disappears. Note that in the 114, 221 and 331 GBs, where the strong local enrichment is accompanied with the depletion near the GB core, the matrix composition does not change after the simulated annealing. Thus, the 111 and 112 GBs can actually accommodate a certain amount of

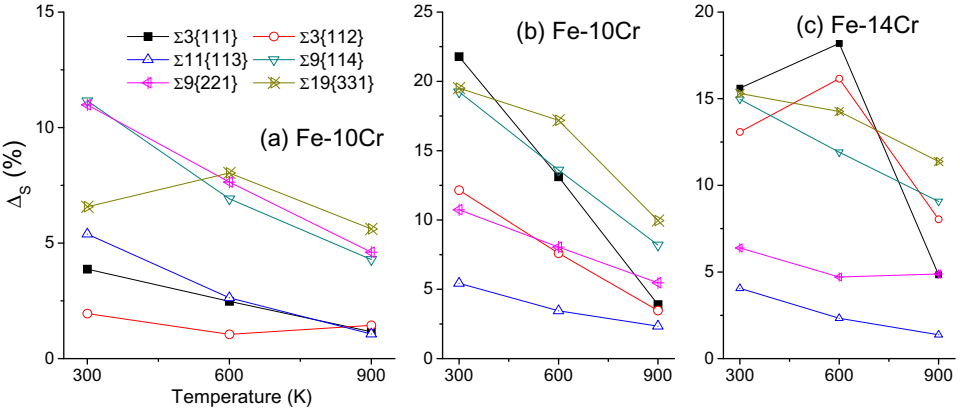


**Fig. 6.** Amount of segregation measured in the GB core after MMC simulations performed in (a) Fe–5Cr, (b) Fe–10Cr and (c) Fe–14Cr bi-crystals.

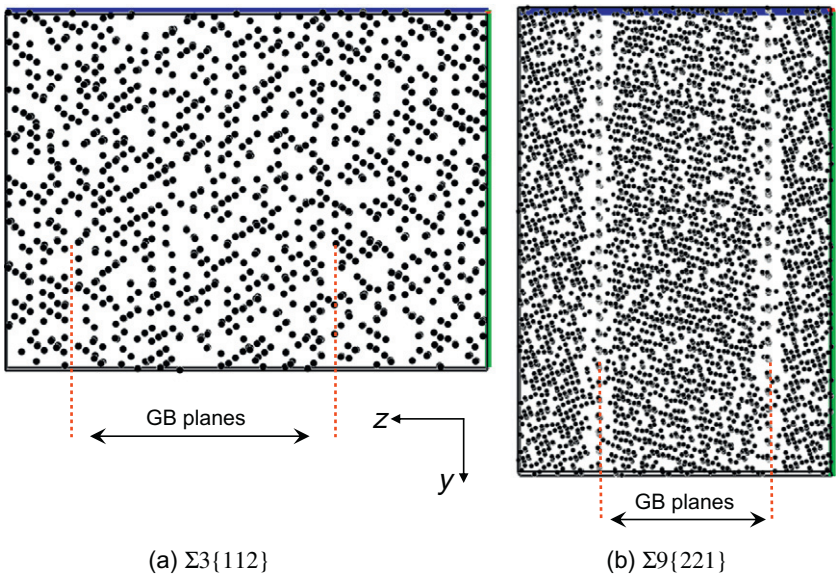


**Fig. 7.** (1 1 0) view on Cr atoms in the Fe–5Cr bi-crystals with (a) Σ3{1 1 2} and (b) Σ9{2 2 1} GBs after MMC simulations performed at 600 K. Traces of the two GB planes are shown for each bi-crystal by dashed lines. The orientation of *z* and *y* axes is also shown.

Cr atoms inside the GB region, while it is only the local rearrangement of the solutes that occurs in the vicinity of the other GBs.

In Fe–14Cr alloy the precipitation of $\alpha'$ occurs at equilibrium according to the applied interatomic potentials up to ~800 K, as was shown by the MMC simulations in the perfect crystals [33]. Despite the fact that some enrichment near the GB core can be seen in the 111, 112, 114, 221 and 331 GBs (see the profiles in Fig. 5), the formation of relatively large Cr precipitates attached to the GB core was observed only in the 111 GB. In the other GBs, Cr precipitates were distributed homogenously in the bi-crystals. This is illustrated in Fig. 8, where Cr clusters (with size >30 atoms, indentified according to the first nearest neighbour distance criterion) formed after the MMC simulations performed at 600 K in the 111 and 114 GBs are shown. Because of the homogenous precipitation, the level of segregation in Fe–14Cr crystals for some GBs is even lower than in Fe–10Cr (see Fig. 6c). The presence of Cr precipitates attached to the interface of the 111 GB was found to cause a slight disturbance of the GB structure. The configuration extracted from the simulations at 300 K is shown in Fig. 9a. However, the visual inspection of the 111 GBs obtained from the simulations at 900 K has shown that the broadening of the GB interface is much stronger than at 300 K and it occurs also in Fe–5Cr and Fe–10Cr (where no $\alpha'$ precipitation was seen at 900 K). Snapshots of the Fe–14Cr and Fe–5Cr crystals equilibrated at 900 K are shown in Fig. 9b and c, respectively. In fact, we can see that the broadening of the GB interface is even wider in Fe–5Cr. We thus conclude that the broadening or movement of the GB interface is not related to the precipitation of Cr clusters but is due to temperature assisted atomic motion. Interestingly to note that the pronounced broadening was observed only in the 111 GB.

### 3.3. Analysis of GB energy

The local atomic rearrangement near the GBs obtained after the MMC simulations may lead to a change in the interface energy. We have therefore calculated the GB energy for the atomic configurations corresponding to the equilibrium states obtained at different temperatures. To do this, the dimensions of the bi-crystals and atomic coordinates were scaled back to the equilibrium lattice unit at 0 K calculated from the zero pressure condition for each alloy composition. These configurations were then fully relaxed using 3D periodic boundary conditions and the GB energy was determined as:

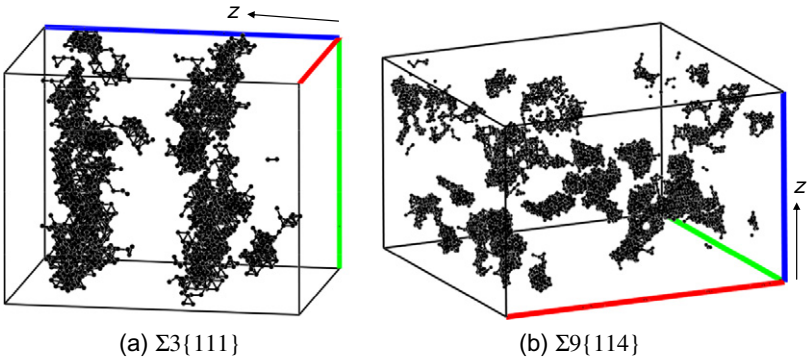


**Fig. 8.** Cr clusters formed in the Fe–14Cr bi-crystals with (a) Σ3{1 1 1} and (b) Σ9{1 1 4} GBs after MMC simulations performed at 600 K. Orientation of the normal to the GB planes is shown by an arrow.

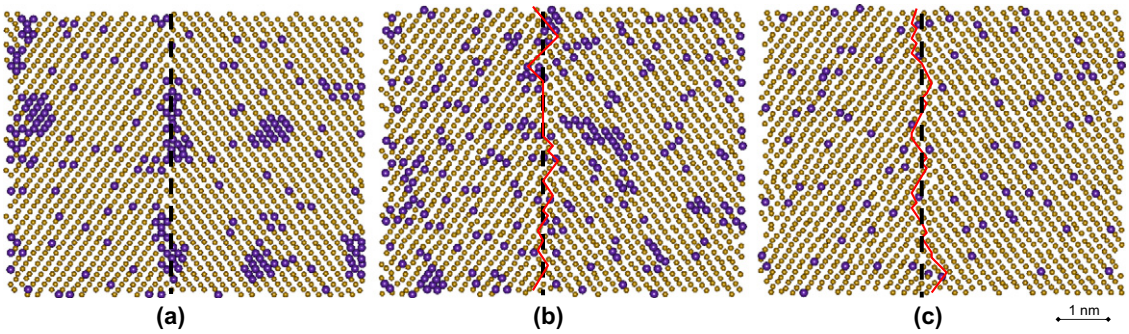


**Fig. 9.** Snapshots showing atoms located in the two non-equivalent (1 1 0) planes of the bi-crystals containing Σ3{1 1 1} GB obtained after MMC simulations performed in (a and b) Fe–14Cr at 300 K and 900 K, respectively, and in (c) Fe–5Cr at 300 K. Dark spheres indicate positions of Cr atoms. The black dashed lines show the trace of the GB plane before the MMC simulations. The red broken lines in figures (b) and (c) show the position of the GB interface after the MMC simulations. (For interpretation of the references to colour in this figure legend, the reader is referred to the web version of this article.)

$$E_{GB} = (E_{SLAB} - E_C \times N_{SLAB})/S_{XY} \quad (3)$$

Here $E_{SLAB}$ is the total energy of the atomic slab with a width of 10 $a_0$ (~3 nm) centered along $z$ axis at the position of the GB interface, $N_{SLAB}$ is the total number of atoms in the slab, $S_{XY}$ is the area of the GB interface and $E_C$ is the cohesive energy of the random alloy with the corresponding composition. Here we note that during the MCC sampling the arrangement of Cr atoms occurs not only at the GB interface but also in the bulk. As a result, the cohesive energy of the bulk atoms also changes. To account for the change of $E_C$ we have calculated the GB energy as

$$E'_{GB} = (E_{SLAB} - E'_C \times N_{SLAB})/S_{XY} \quad (4)$$

where $E'_C$ is the average cohesive energy calculated in a perfect Fe–Cr crystal (containing 16,000 atoms) after the MMC simulations performed at 300 K.

First we present the GB energy as a function of GB orientation calculated for the random alloys in the configurations that were used for the subsequent MMC simulations. The GB energy for pure Fe and the three alloys are shown in Fig. 10a. The alloying of iron by Cr does not lead to a strong change in the GB energy and the difference stays within 15% for all GBs and compositions studied. The weak effect of Cr alloying on the GB energy observed here correlates well with recent results obtained by Shibuta et al. [34], who used another EAM potential to study cohesive properties of ⟨1 1 0⟩ symmetric tilt boundaries. In the following, we shall restrict the analysis to consider only the configurations obtained at 300 K, as the strongest Cr rearrangement was seen at this temperature. We shall also exclude configurations obtained in the Fe–14Cr bi-crystals because of the $\alpha$–$\alpha'$ phase separation that occurred after the MMC simulations. In this case we cannot use cohesive energy of the random alloy as a reference state to calculate the GB energy. In the case of Fe–5Cr alloy, the short range ordering of Cr in the bulk decreases the cohesive energy by about ~3 meV/atom (see also Ref. [33]), according to the applied here potential. The decrease of the cohesive energy in Fe–10Cr alloy after MMC simulations at 300 K is ~1 meV/atoms.

The GB energy for Fe–5Cr and Fe–10Cr calculated in the crystals obtained from the MMC simulations at 300 K is shown in Fig. 10b and c, respectively. The data for pure Fe and the corresponding random alloys are added for comparison. Clearly, the rearrangement of Cr in the GB core results in the decrease of $E_{GB}$. However, the decrease of the GB energy comes not only from the refinement of Cr at the GB interface but also is due to the rearrangement in the bulk. To account for the change of the bulk cohesive energy we also draw $E'_{GB}$, calculated using Eq. (4). We see that the interface energy calculated using. Eq. (4) is still lower than that in pure Fe and in random alloys. Note that the decrease of $E_{GB}$ occurred even in the 112 GB in the Fe–5Cr bi-crystals, where no clear enrichment or depletion of Cr was registered. It means that the Cr rearrangement in this GB is expressed in the local ordering and refinement of energetically unfavourable sites for the solutes. To quantify the possible ordering in the Fe–5Cr alloys we have calculated the SRO parameter using the Warren–Cowley expression [8]. The SRO parameter, $\eta_v^A$, in the $v$-th nearest neighbour shell for a representative atom of type $A$ in a binary $AB$ alloy is defined as:

$$\eta_v^A = 1 - \frac{p^v(B|A)}{x_B} \quad (5)$$

where $p^v(B|A)$ denotes the probability of finding an atom of type $B$ in the $v$-th nearest neighbour shell of an atom of type $A$; $x_B$ denotes the

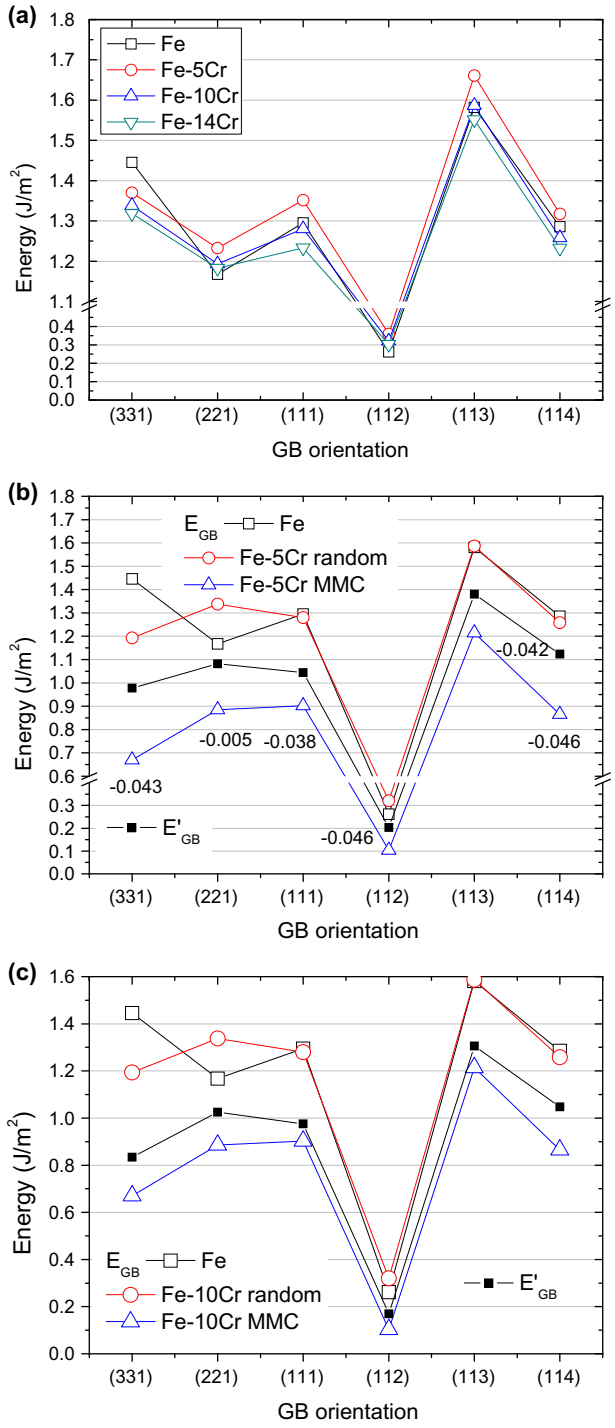


**Fig. 10.** GB energy calculated in (a) the random Fe–Cr alloys, (b) Fe–5Cr and (c) Fe–10Cr after MMC simulations performed at 300 K. The values of the SRO parameter calculated in Fe–5Cr bi-crystals are also given in figure (b). The interface energy $E_{GB}$ and $E'_{GB}$ are calculated using Eqs. (3) and (4), respectively.

overall concentration of atoms of type *B*. Physically, $\eta_v^A$ measures the deviation from the random state at a short distance and $\eta_v^A = 0$ corresponds to the random state. Here we used the second nearest neighbour distance (i.e., $a_0$) to calculate $\eta_v^A$. The values are reported in Fig. 10b. We can see that in all bi-crystals $\eta_v^A$ is negative and is close to the lowest possible value for the studied concentration (which is −0.052). We do not see any clear correlation between the Cr concentration profiles, which essentially differ (see Fig. 3), and SRO parameter being nearly the same for all GBs. $\eta_v^A$ calculated for the first and third *n* shell did not show any clear trend either. Hence, we conclude that the main contribution to the SRO parameter comes from the bulk where the established ordering is the same in all bi-crystals and is not influenced by the presence of the GB interface.

## 4. Summary

In this work, we have carried out an atomistic study of rearrangement in Fe–Cr alloys considering several different tilt symmetric grain boundaries. The calculations have been performed using MS and MMC techniques by applying a set of recently developed interatomic potentials for Fe–Cr, partially fitted to *ab initio* data.

Results of the static simulations suggest that all considered GBs have energetically preferential sites for substitutional Cr atoms, but the actual binding energy depends significantly on the GB structure. The interaction is highly non-uniform in the GB core, especially in the GBs with high Σ. Thus, the two adjacent atomic positions in the core can be preferential and unfavourble sites for substitutional Cr. It is therefore difficult to make any definitive conclusion regarding the rearrangement of Cr in concentrated alloys relying only on the results of MS simulations, especially keeping in mind the presence of a strong Cr–Cr repulsion in the first nearest neighbour positions [35] which can play an important role in the multi-body interaction. Note that the Cr–Cr repulsion in bulk Fe and the heat of mixing of the Fe–Cr system is adequately reproduced by the applied here potentials, taking the *ab initio* data as reference [36]. Hence, the rearrangement of Cr atoms in concentrated random Fe–Cr alloys at equilibrium was studied using the MMC techniques.

The enrichment of the central part of the GB core was found in the most of the performed simulations, irrespective of temperature and alloy composition. However, the enrichment in the GBs with high Σ (i.e., Σ19{3 3 1}, Σ11{1 1 3}, Σ9{1 1 4} and Σ9{2 2 1}) is found to be more pronounced, which is consistent with a relatively high binding energy found from static simulations. In addition, the strong depletion of Cr in the outer part of the core of these GBs was found in Fe–5Cr and Fe–10Cr alloys (see Figs. 3 and 4). This again seems to be consistent with the presence of unfavourable sites for a substitutional Cr located near the core (see Fig. 2). The mentioned simultaneous local enrichment and depletion is, however, only a result of the rearrangement of Cr, while the concentration of Cr in the matrix essentially did not change after the MMC runs. Actual Cr segregation was observed only in Fe–10Cr in the Σ3{1 1 1} and Σ3{1 1 2} GBs, where a considerable Cr depletion of the matrix was registered (see Fig. 4). This result shows that the equilibrium segregation in the studied system depends not only on the GB structure and temperature but also on the ambient composition. From this view point no clear correlation between the results of the static calculations (characterizing the interaction of Cr atom(s) in pure Fe matrix) and MMC simulations (performed in concentrated alloys) can be established.

Even though, a local Cr concentration measured at the GB interface in Fe–5Cr and Fe–10Cr alloys essentially exceeds the solubility limit at the studied temperatures, no Cr precipitates were seen to form. We explain this by the fact that this enrichment is actually confined in one or two interatomic planes, while outside the depletion takes place.

The local enrichment was accompanied by a certain atomic disorder within a few atomic planes around the GB core. The width of the disordered GB region tends to increase with increasing temperature and is not seen to correlate with the formation of Cr precipitates on the GB interface. In other words, the presence of Cr precipitates in the GB core does not produce as strong disorder

as temperature itself. At this, the degree of the temperature induced disorder depends significantly on the structure of a particular GB. The interface of the GBs with high Σ has shown very good resistance to the disorder with increasing temperature up to 900 K. Whereas, a front of the Σ3{1 1 1} was found to move already at 600 K. Hence, the thermal stability of tilted GBs and factors affecting it should be addressed and it will be studied in our future work. Another important effect of temperature in the MMC simulations was expressed in the suppression of the local enrichment and depletion seen in the GB region, which is expected. Finally, with increasing temperature the distribution of Cr precipitates in the Σ3{1 1 1} in Fe–14Cr changes from a heterogeneous, when large Cr clusters were attached to the GB core, to the uniform one.

The GB energy estimated in the crystals obtained from the MMC simulations at 300 K was found to be lower than in random alloys or in pure Fe. Typically, the GB energy and ideal cleavage energy are correlated. It is, however, too early to make a conclusion that the decrease of $E_{GB}$ in these alloys enhances their strength with respect to fracture. First of all, the definition of ideal cleavage energy also includes the energy of the free surface to be formed in the cleavage process. At this point we do not know how the surface energy is affected by the Cr redistribution near the GB core. Secondly, in our recent atomistic study of the cleavage fracture in pure Fe we have shown that the GB fracture process involves movement of a GB front accompanied by sliding. Given that the resistance of a grain boundary to sliding is closely related to its structure, one needs to investigate the effect of local Cr rearrangement on the GB sliding.

At the end this section let us point out several challenges of the atomistic techniques applied here to describe properties of grain boundaries in concentrated alloys. First of all, the accuracy of the cohesive model is one of the pillars of any atomistic study whose results can be considered as reliable ones. Atomistic modeling of Fe–Cr alloys has been a very active area of research during the last decade and from that viewpoint the two band EAM interatomic potential applied here [20] has been benchmarked extensively (see references in the introduction) and generally is found to provide satisfactory agreement with existing experimental and *ab initio* data. Yet, many structural properties (and anomalies) in the Fe–Cr system have complex magnetic origin, which could hardly be described by central force potentials as accurately as *ab initio* methods do.

Clearly, further validation of the results of static simulations obtained here is necessary. However, *ab initio* techniques can deal only with very small supercells (up to a few hundreds of atoms). Whereas, the smallest periodic supercell (for which the box-size effect is not important) for some of the GBs considered here contains already more than one thousand atoms. GBs with a simple periodic structure such as Σ3(1 1 1), Σ3(1 1 2) and Σ5(0 1 3) can indeed be modeled using *ab initio* methods, but again due to the limitation of the box-size, only relatively high surface concentration of solutes can be considered. In this case the effect of self-interaction via periodic boundary remains unknown.

One also needs to note that we deal with idealized symmetric GBs constructed following the coincidence lattice site methodology. While up to now not much is known about actual atomic structure of high angle grain boundaries in bcc Fe and Fe-based alloys. The local equilibrium configurations represent states that in principle may be produced during the evolution of the system under thermal annealing. However, the applied MMC technique does not sample atomic path and therefore no information about time involved to establish the final state is available. Yet, the equilibrium states obtained here can serve as indication for the trends to be expected from the results obtained by kinetic methods.

Finally, we note that a direct comparison of the Cr profiles near GB obtained here with those measured experimentally under irradiation conditions is not appropriate, as in the case of irradiation the solute concentration gradient may appear as a result of the non-equilibrium segregation. As observed experimentally, the broadening of the peak due to Cr enrichment (or sometimes depletion) at a grain boundary in Fe–Cr alloys and high-Cr ferritic steels is of the order of tens of nanometers [8,37]. Whereas the enrichment observed in the present calculations is essentially confined in a few interatomic planes.

## 5. Conclusions

Based on the results presented above we can draw the following conclusions:

(1) The binding energy of a substitutional Cr to the GB core is essentially determined by the structure of the GB interface. The strongest binding energy (~0.3 eV) is found for GBs with the largest excess volume, such as Σ9{2 2 1} and Σ9{1 1 4} GBs. The weakest interaction takes place in the Σ3{1 1 2} GB.
(2) All considered GBs contain both energetically preferential and unfavourable sites for the segregation of Cr. At this, the most preferential sites are usually located in the plane coinciding with the actual GB interface, while the unfavourable sites are in the close neighbouring planes. A total number of preferential and unfavourble sites (per unit area) depends significantly on the core structure.
(3) The performed MMC simulations reveal that in the Fe–5Cr bi-crystals a clearly distinguished enrichment of the GB core by Cr takes place in all GBs except for the Σ3{1 1 2}. In all the considered GBs, no matrix depletion was found.
(4) In Fe–10Cr, a pronounced depletion of Cr in the matrix and enrichment in the GB region is found in the bi-crystals containing Σ3{1 1 1} and Σ3{1 1 2} GBs.
(5) In Fe–14Cr, the preferential precipitation of α' particles was found at the interface of the Σ3{1 1 1} GB only. The spatial distribution of Cr precipitates becomes homogenous in the bi-crystal containing the Σ3{1 1 1} GB with increasing temperature. Homogenous precipitation was seen in the rest of the studied GBs.
(6) The effect of temperature is: (i) to weaken the enrichment of the GB core in Fe-5 and Fe–10Cr; (ii) to diminish the matrix depletion in Fe–10Cr; (iii) to induce homogenous distribution of precipitates in the bi-crystals in Fe–14Cr; (iv) to cause the displacement/broadening of the interface of the Σ3{1 1 1} GB.
(7) The GB energy measured in Fe-5 and Fe–10Cr after the MMC simulations is found to be lower than in the corresponding random alloys and pure Fe.

## Acknowledgements

This work was performed in the framework of the seventh Framework Programme collaborative project GETMAT, partially supported by the European Commission, Grant agreement number 212175. XH acknowledges National Natural Science Foundation of China, Grant number 10975194; National Basic Research Program of China, Grant number 2007CD209801. Part of the calculations was performed at the supercomputer facilities JUROPA within the APM project.

## References

[1] A. Sutton, R. Balluffi, Interfaces in Crystalline Materials, Oxford Science Publications, New York, 1995.
[2] B. Kempshall, B. Prenitzer, L. Giannuzzi, Scripta Mater. 47 (2002) 447.

[3] M. Menyhard, M. Yan, V. Vitek, Acta Metall. Mater. 42 (1994) 2783.
[4] X. Xie, Y. Mishin, Acta Mater. 50 (2002) 4303.
[5] S. Jitsukawa, A. Kimura, A. Kohyama, R.L. Klueh, A.A. Tavassoli, B. van der Schaaf, G.R. Odette, J.W. Rensman, M. Victoria, C. Petersen, J. Nucl. Mater. 329–333 (2004) 39.
[6] R. Lagneborg, Trans. ASM 60 (1967) 67.
[7] H. Takahashi, S. Ohnuki, T. Takeyama, J. Nucl. Mater. 103–104 (1981) 1415.
[8] T. Muroga, M. Yoshida, K. Kitajima, Ultramicroscopy 22 (1987) 281.
[9] T. Ezawa, T. Akashi, R. Oshima, J. Nucl. Mater. 212–215 (1993) 252.
[10] Z. Lu, R. Faulkner, G. Was, B. Wirth, Scripta Mater. 58 (2008) 878.
[11] P. Olsson, I. Abrikosov, L. Vitos, J. Wallenius, J. Nucl. Mater. 321 (2003) 84.
[12] R. Fisher, E. Dulis, K. Carroll, Trans. Metall. Soc. AIME 197 (1953) 690.
[13] R. Williams, H. Paxton, J. Iron Steel Inst. 185 (1957) 358.
[14] I. Mirebeau, M. Hennion, G. Parette, Phys. Rev. Lett. 53 (1984) 687.
[15] N. Metropolis, A. Rosenbluth, M. Rosenbluth, A. Teller, E. Teller, J. Chem. Phys. 21 (1953) 1087.
[16] M. Allen, D. Tildesley, Computer Simulation of Liquids, Clarendon Press, Oxford, 1987.
[17] E.E. Zhurkin, R. Pereira, N. Castin, L. Malerba, M. Hou, Mater. Res. Soc. Symp. Proc. 1125 (2009) 121.
[18] K. Binder, Monte Carlo Methods in Statistical Physics, Springer-Verlag, Berlin, 1979.
[19] D. Terentyev, X. He, A. Serra, J. Kuriplach, Comput. Mater. Sci. 49 (2010) 419.
[20] P. Olsson, J. Wallenius, C. Domain, K. Nordlund, L. Malerba, Phys. Rev. B 72 (2005) 214119.
[21] D. Terentyev, M. Klimenkov, L. Malerba, J. Nucl. Mater. 393 (2009) 30.
[22] K. Vörtler, C. Björkas, D. Terentyev, L. Malerba, K. Nordlund, J. Nucl. Mater. 382 (2008) 24.
[23] C. Björkas, K. Nordlund, L. Malerba, D. Terentyev, P. Olsson, J. Nucl. Mater. 372 (2008) 312.
[24] D. Terentyev, G. Bonny, L. Malerba, Acta Mater. 56 (2008) 3229.
[25] D. Terentyev, G. Bonny, L. Malerba, J. Nucl. Mater. 386–388 (2009) 257.
[26] G. Bonny, D. Terentyev, L. Malerba, D. Van Neck, Phys. Rev. B 79 (2009) 104207.
[27] G. Ackland, M. Mendelev, D. Srolovitz, S. Han, A. Barashev, J. Phys. Condens. Matter 16 (2004) 1.
[28] F. Willaime, C. Fu, M. Marinica, J. Dalla Torre, Nucl. Instrum. Methods Phys. Res. B 228 (2005) 92.
[29] C. Domain, G. Monnet, Phys. Rev. Lett. 95 (2005) 215506.
[30] D. Terentyev, P. Olsson, T. Klaver, L. Malerba, Comput. Mater. Sci. 43 (2008) 1183.
[31] E. Wachowicz, T. Ossowski, A. Kiejna, Phys. Rev. B 81 (2010) 094104.
[32] G. Bonny, D. Terentyev, L. Malerba, Scripta Mater. 59 (2008) 1193.
[33] E.E. Zhurkin, R. Pereira, N. Castin, L. Malerba, M. Hou, Mater. Future Fusion Fission Technol. 1125 (2009) 121.
[34] Y. Shibuta, S. Takamoto, T. Suzuki, Comput. Mater. Sci. 44 (2009) 1025.
[35] T. Klaver, P. Olsson, M. Finnis, Phys. Rev. B 76 (2007) 214110.
[36] L. Malerba, A. Caro, J. Wallenius, J. Nucl. Mater. 382 (2008) 112.
[37] S. Ohnuki, H. Takahashi, T. Takeyama, J. Nucl. Mater. 122–123 (1984) 317.